Response of low quartz SiO_2 to the presence of an external static electric field: A density functional theory study

Moussab Harb, Pierre Labéguerie, Isabelle Baraille, and Michel Rérat*

Institut Pluridisciplinaire de Recherche sur l'Environnement et les Matériaux, UMR CNRS 5254, Université de Pau et des Pays de l'Adour, Hélioparc Pau-Pyrénées, 2 Avenue du président Pierre Angot, 64053 Pau Cedex 9, France

(Received 22 July 2009; revised manuscript received 5 October 2009; published 29 December 2009)

We present a systematic theoretical study of response properties of α-quartz SiO_2 to an external static electric field in the framework of the density functional theory. The distortions of the electron density and crystalline structure by the application of the field are investigated and compared to x-ray scattering intensity variations obtained by Guillot *et al.* when a macroscopic electric field of 28.8 kV/cm is applied along the crystallographic *a* axis. Our calculations show that the experimental macroscopic field produces mainly atomic displacements, with a negligible electronic contribution. The calculated displacements along the *a* axis are in good agreement with the experimental data obtained from structure factors while the perpendicular displacements are found to be smaller, as well as the rotations of the Si-O bonds in the two independent tetrahedra around the *a* axis. In this work, the direct gap, the high-frequency dielectric constant as well as the elastic and piezoelectric tensors are also computed in order to confirm the accuracy of our calculations.

DOI: 10.1103/PhysRevB.80.235131 PACS number(s): 71.10.−w, 71.20.Nr, 77.65.−j, 77.84.−s

I. INTRODUCTION

α quartz has a trigonal crystalline structure containing three SiO_2 in its unit cell in the $P3_221$ or $P3_121$ symmetry space groups (left and right handed, respectively). Its structure is formed of corner-sharing SiO_4 tetrahedra. It is the most stable silica polymorph at ambient conditions (up to 3 GPa), and persists as a metastable state at higher pressures. Quartz amorphizes at pressures of around 18–35 GPa.[1–3] On the release of pressure, quartz remains amorphous[1] but is anisotropic with the memory of the quartz crystallographic orientation.[4]

α-quartz SiO_2 is the most widely used piezoelectric material until present. For the last ten years, it has been the subject of many experimental[5–11] and theoretical[12–15] studies which have focused on the determination of its structural, electronic, elastic, and piezoelectric properties. Since the discovery of piezoelectric effect by the Curie brothers in 1880,[16] its moderate piezoelectricity, high-temperature stability of resonance frequencies, and low internal friction have provided a large variety of applications such as filters, oscillators, sensors, electronic watches, computers, cellular phones, etc.

However, the origin of the piezoelectric properties and the polarization is not clear. Pure ionic displacements of the Si^{4+} and O^{2-} sublattices (i.e., the Meissner model[17]) cannot explain these properties as the Si-O bonds are known to be partially covalent. Beyond the ionic model, according to many studies,[18–21] the origin of the polarization could be described by a change in the bridge angle between the SiO_4 tetrahedra which were rotated as rigid objects against each other. However, the small variations reported for the bond angles would not explain the order of magnitude of the experimental piezoelectric response. The direct investigation at the atomic level of the structural distortions induced by an applied electric field should help to clarify the relevance of the structural contributions to these piezoelectric properties.

Beyond this scope, an x-ray diffraction study has been carried out in 2004 by Guillot *et al.*[8] on α quartz in presence of a macroscopic electric field of 28.8 kV/cm applied in the direction of the crystallographic *a* axis. They have measured the effect of a static electric field on the structure factors. The atomic displacements of Si and O atoms along the three Cartesian axes, as well as the rotations of the Si-O bonds around these axes, the angles in the unperturbed and perturbed structures, the angles between the Si-O bonds and the electric field direction have been then deduced from a charge-density model. The analysis has indicated that the bond distances Si-O are very little affected by the field but both a deformation and a reorientation of the SiO_4 tetrahedra have been observed.

In this work, we report the first *ab initio* calculations of atomic displacements induced by the presence of a strong external field in order to deduce the response properties of the α quartz. The evolution of the electron density and the structural distortion of α-quartz SiO_2 is investigated as a function of the applied electric field amplitude in the framework of the density functional theory (DFT). The different measured elements given in Ref. 8 have been calculated in order to give relevant additional information. The derivatives of the energy with respect to strain and electric field such as the elastic, piezoelectric, and dielectric tensors have been also calculated at fixed geometry in order to confirm the accuracy of our wave-function calculations.

II. METHOD AND COMPUTATIONAL DETAILS

The linear combination of atomic orbitals (LCAO)-DFT periodic calculations were performed using the CRYSTAL06 (Ref. 22) package developed in Torino. The crystalline orbitals are expanded in terms of localized atomic Gaussian basis set, in a way similar to the LCAO method currently adopted for molecules. The eigenvalues equations are solved using both the nonlocal generalized gradient approximation (GGA) approach developed on the Perdew-Wang (PW) functionals[23–25] and the B3LYP functional based on the Becke's three parameters adiabatic connection exchange

TABLE I. Optimized unit-cell parameters (Å), volume (Å^3), direct gap (eV), fractional coordinates and Si-O bonds (Å). For the unit-cell parameters and the Si-O bonds, the percentage errors given in parenthesis are compared to experimental data (Refs. 8 and 11). For the direct gap, the results are compared to experimental data given in Ref. 9.

	AE-B3LYP	AE-PWGGA	PS-B3LYP	PS-PWGGA	Expt.
a	4.976 (2%)	4.956 (1%)	4.938 (1%)	4.919 (0.2%)	4.910[a]
c	5.487 (2%)	5.481 (2%)	5.434 (1%)	5.425 (0.5%)	5.401[a]
V	117.69 (2%)	116.63 (4%)	114.76 (2%)	113.76 (1%)	112.76[a]
x_{Si}	0.468	0.465	0.468	0.465	0.470[b]
x_O	0.413	0.410	0.413	0.409	0.413[b]
y_O	0.270	0.276	0.275	0.269	0.267[b]
z_O	0.117	0.111	0.117	0.111	0.119[b]
Si-O_1	1.618 (0.6%)	1.642 (2.2%)	1.632 (1.5%)	1.628 (1.3%)	1.607[b]
Si-O_2	1.623 (0.6%)	1.646 (2%)	1.636 (1.4%)	1.632 (1.2%)	1.613[b]
Gap	8.7	6.3	10.3	7.6	9.2[c]

[a]Reference 8.
[b]Reference 11.
[c]Reference 9.

functional[26] in combination with the Lee-Yang-Parr's correlation functional.[27] The number of k points in the first irreducible Brillouin zone in which the Hamiltonian matrix is diagonalized, is equal to 65. All-electron (AE) basis sets (6-21G* for silicon[28] and 8-41G* for oxygen[29]) were used for orbital expansion solving the Kohn-Sham equation iteratively. We set the total-energy tolerance to 10^{-9} hartree and eigenvalue tolerance to 10^{-8} hartree in the iterative solution of the Kohn-Sham equations. The level of accuracy in evaluating the Coulomb series is controlled by five parameters, for which standard values given in CRYSTAL (i.e., 6 6 6 6 12) have been used. Vibration frequencies analysis was performed to guarantee that optimized structures are local minima.

In order to reduce the computational cost, the Durand and Barthelat effective core pseudopotentials[30] (PS) are also used to model the core electrons in oxygen and silicon atoms. Valence basis sets (PS-2-1-1G* for silicon and PS-4-1G* for oxygen) (Ref. 31) which were already optimized in early studies with respect to the description of SiO_2 bulk structures of rutile and cristobalite are adopted.

For the electrical part, the calculation of response properties (high-frequency dielectric constant and distortion of crystalline structures) to an external static electric field was carried out by the finite-field (FF) perturbation method implemented in CRYSTAL06.[22] In order to maintain the periodicity along the applied field direction, a triangular electric potential is used in conjunction with a $(4\times1\times1)$ supercell to guarantee a response field constant in the middle of each half supercell.[32] Besides, the dipolar moment locally induced by the applied field in a plane of crystal can be also reproduced.

Using the analytical gradient of the potential including the field perturbation, the crystalline structures in the presence of an applied external field have been optimized. Very small variations in the lattice parameters of $(4\times1\times1)$ supercell in the presence of the field were found. Note that the electric field $\vec{F}$ used experimentally corresponds to a macroscopic field (seen by atoms) while the finite field $\vec{F}_0$ incorporated into the self-consistent field calculations corresponds to a displacement field. The field $\vec{F}_0$ is larger than the one seen by atoms since the electronic polarization $\vec{P}$ generated in the crystal is included ($\vec{F}_0=\vec{F}+\vec{P}/\varepsilon_0$, where ε_0 represents the vacuum permittivity).

For the determination of elastic and piezoelectric coefficients, the six nonzero independent components of the elastic tensor found for the α quartz, namely, C_{11}, C_{12}, C_{13}, C_{14}, C_{33}, and C_{44} have been computed by fitting the total energy as a function of the applied strain while the two nonzero independent components of the piezoelectric tensor, namely, e_{11} and e_{14} have been computed by fitting the three Berry's phase components φ_1, φ_2, and φ_3 as a function of the applied strain on the unit cell.[33] Besides, 11 values for the strain in the interval $[-0.020,\ +0.020]$ were considered for the fitting, and the deformation of the unit cell by the strain was carried out within a constant volume. The details of the methods used to compute the elastic and piezoelectric coefficients may be found in CRYSTAL06.[22]

III. RESULTS AND DISCUSSIONS

A. Structural and electronic properties

We have optimized the crystalline structure of α-quartz SiO_2 starting from the lattice parameters obtained experimentally by Guillot *et al.*[8] Four approaches: AE-B3LYP, AE-PWGGA, PS-B3LYP, and PS-PWGGA have been investigated. The results for the optimized atomic positions and the unit-cell parameters as well as the corresponding experimental data, are reported in Table I. A summary of the main interatomic bonds (namely, Si-O_1 and Si-O_2) and the direct gap are also given. Our calculations for the lattice parameters show that both AE approaches give overestimated values by 1–2 % compared to the experimental ones. For the Si-O

TABLE II. Elastic (GPa) and piezoelectric (C/m^2) coefficients. Comparison with the experimental data (Ref. 5); at two temperatures: 275 K (in the left) and 5 K (in the right) and (Ref. 6) at 303 K.

		AE-B3LYP	PS-B3LYP	PS-PWGGA	Expt. (Ref. 5)	Expt. (Ref. 5)	Expt. (Ref. 6)
C_{ij} (GPa)	C_{11}	89.73	94.00	86.30	86.76	86.56	86.76
	C_{12}	12.83	13.11	18.25	7.06	9.42	6.86
	C_{13}	16.37	17.81	18.04	11.90	12.80	11.85
	C_{14}	−14.76	−15.98	−13.98	−17.98	−17.83	−18.02
	C_{33}	112.02	112.90	115.90	105.41	107.65	105.5
	C_{44}	57.89	60.05	57.61	58.27	59.60	58.14
	C_{66}	38.45	40.44	34.02	39.85	39.12	39.95
e_{ij} (C/m^2)	e_{11}	0.184	0.164	0.176	0.149	0.066	0.151
	e_{14}	−0.055	−0.054	−0.069	−0.057	−0.026	−0.061

bonds, our results show a good agreement for the AE-B3LYP approach with the experiment (0.6%) whereas the values given by the PWGGA method are larger than the experimental data by 1.2–1.3 %. The results for the gap given in Table I clearly confirm the well-known ability of the hybrid exchange-correlation functional B3LYP to provide band gap close to experimental data.[34] This is not the case for the AE-PWGGA approach for which an underestimated value of 2.83 eV is obtained. As the response properties investigated in this work are second- and third-order properties which strongly depend on the gap, we rule out afterward the AE-PWGGA approach. The PS results differ slightly respected to the corresponding AE values at both B3LYP and PWGGA levels. The lattice parameters are systematically shorter by 1% and the band gap is increased by 1.3 or 1.6 eV. Surprisingly, the PS-PWGGA approach gives the best agreement with the experimental lattice parameters and a relatively good agreement for the gap. This is fortuitously due to errors that counterbalance. As the response properties investigated in this work are second- and third-order properties which strongly depend on the gap, we rule out the AE-PWGGA approach, in the following.

B. Elastic and piezoelectric tensors

Elastic and piezoelectric tensors of materials can be obtained by applying a strain tensor (η_{kl}) on the unit cells. The elastic response tensor is represented by the second-order derivative of total energy with respect to applied strain tensor components. It is a four-rank tensor, $C_{klmn}=\frac{1}{V_0}\left[\frac{\partial^2 E}{\partial \eta_{kl}\eta_{mn}}\right]_0$, where V_0 is the equilibrium volume of the unit cell and k, l, m, and $n=1-3$ are Cartesian indexes. The piezoelectric response tensor is indicated by the property of some crystals to generate (or to acquire) an electric polarization under the influence of mechanical effort, such as compression or traction. It is represented by the first-order derivative of generated electric polarization components with respect to applied strain tensor components. It is a three-rank tensor, $e_{ikl}=\left[\frac{\partial P_i}{\partial \eta_{kl}}\right]_0$ with i, k, and $l=1$, 2, and 3. Note also that the crystals which own a symmetry center cannot have piezoelectric properties.

Following this, we have calculated the elastic and piezoelectric coefficients (C_{ij} with $i,j=1-6$ and e_{ij} with $i=1-3$ and $j=1-6$ using Voigt's notation) of the α-quartz SiO_2 within the AE-B3LYP, PS-B3LYP, and PS-PWGGA approaches. The main goal is to study at the same time the effect of the basis sets and the exchange-correlation functional on the elastic and piezoelectric coefficients. The results are shown in Table II. By comparing the different values obtained under the three approaches, our calculations show a weak effect of the exchange-correlation functional and of the basis sets on the elastic and piezoelectric coefficients. The three approaches give results in good agreement with the experimental values obtained at 275 and 5 K (Ref. 5) and also at 303 K,[6] except for nondiagonal component C_{12}. This discrepancy is probably due to a temperature effect which is not taken into account in this approach.[5]

C. Response properties to an external static electric field

1. High-frequency dielectric tensor

After having calculated the direct gap and the elastic and piezoelectric coefficients with different theoretical approaches, we have calculated the response properties of α-quartz SiO_2 to an external field in the framework of the FF method, by keeping only the AE-B3LYP and PS-PWGGA approaches, for which a good agreement with the experiment is established. Starting from the optimized lattice parameters of the unit cell and applying an external electric field of 5×10^{-3} a.u. along the three Cartesian axes (x, y, and z), we have calculated the three nonzero components ($\varepsilon^{\infty}_{xx}$, $\varepsilon^{\infty}_{yy}$, and $\varepsilon^{\infty}_{zz}$) of the high-frequency dielectric tensor using the following formula: $\varepsilon_{ii}=\frac{F_{0i}}{F_i}=\frac{F_{0i}}{F_{0i}-P_i/\varepsilon_0}$, where the polarization vector is obtained from Poisson's equation and the perturbed electron density.[32] The component values obtained with the PS-PWGGA approach are equal to those obtained with AE-B3LYP ($\varepsilon^{\infty}_{xx}=\varepsilon^{\infty}_{yy}=2.22$ and $\varepsilon^{\infty}_{zz}=2.26$) in good agreement with the available experimental values[10] ($\varepsilon^{\infty}_{xx}=\varepsilon^{\infty}_{yy}=2.24$ and $\varepsilon^{\infty}_{zz}=2.27$). Since the calculation of the dielectric constant mainly depends on the number of valence electrons, the use of a PS in our calculations aims at reducing the time of calculation in order to study other typical compounds having many valence electrons such as $FePO_4$, $GaPO_4$, and $GaAsO_4$.

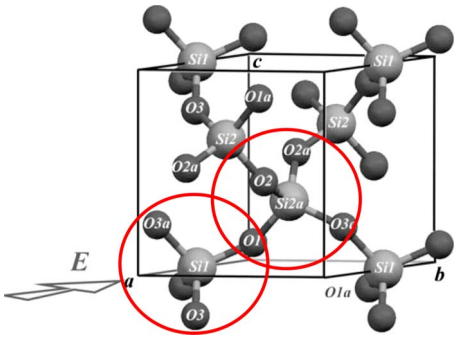

FIG. 1. (Color online) Perspective view of the α-quartz structure. The two independent tetrahedra centered at Si_1 and Si_{2a} following the notation of Guillot *et al.* (Ref. 8) are surrounded.

2. *Effect of the external electric field on the electron density*

The aim of this section is to calculate the electron density of the quartz induced by an external electric field for a given nuclei configuration, in order to evaluate the electronic contribution to the response of SiO_2 to an applied field. As previously announced, the presence of an external electric field described by a triangular potential led us to use a $(4\times1\times1)$ supercell with a symmetry group space C_2 (as the experimental one) in order to correctly calculate the response of the crystal to an electric field with the FF method. Since the applied field is not constant everywhere in the supercell, we have selected the atoms in the area of the constant response field. The electric field being applied parallel to one of the twofold rotation axes, the deformed structure will have the space-group symmetry C_2. However, we keep describing the atomic positions in the primitive unit cell obtained directly from the original hexagonal cell as illustrated in Fig. 1. This figure also displays the labels of the atoms. In the perturbed structure, there are two symmetrically independent silicon atoms, one on the twofold rotation axis (labeled Si_1) and the other being at a general position (labeled Si_2). The origin of the cell is fixed by the Si_1 position; its coordinates are therefore not refined. Among the six oxygen atoms in the unit cell, three are symmetrically independent in the deformed structure. A total of 12 parameters must therefore be refined to describe the atomic displacements under the influence of the electric field. For different applied field amplitudes $F_0=10^{-2}$, 5×10^{-3}, and 10^{-3} a.u. (1 a.u. of field amplitude$=5.1\times10^6$ kV/cm), we have analyzed the evolution of the electron density around two types of Si-O bonds in the deformed structure. Following this, Figs. 2 and 3 associated at two planes (010) containing the Si_1-O_1 and Si_{2a}-O_{3a} bonds, respectively, report the difference electron-density maps between the total charge density associated at $\vec{F}_0=\vec{0}$ and the one corresponding to $\vec{F}_0\neq\vec{0}$ using the AE-B3LYP approach.

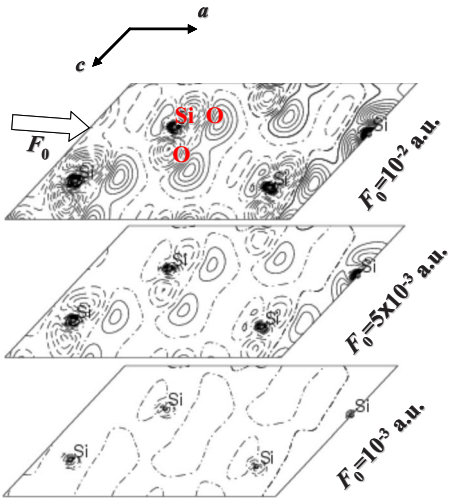

FIG. 2. (Color online) Difference electron-density maps between the total charge densities of the perturbed (α−quartz+field) and unperturbed systems on a plane containing the Si_1-O_1 bond for three different electric field amplitudes: 10^{-2}, 5×10^{-3}, and 10^{-3} a.u. The dotted lines are negative and the full lines are positive. Isovalue is 0.0001 bohr^{-3}.

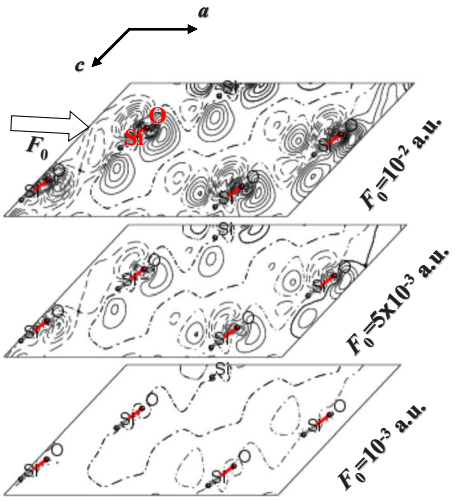

FIG. 3. (Color online) Difference electron-density maps between the total charge densities of the perturbed (α−quartz+field) and unperturbed systems on a plane containing the Si_{2a}-O_{3a} bond for three different electric field amplitudes: 10^{-2}, 5×10^{-3}, and 10^{-3} a.u. The dotted lines are negative and the full lines are positive. Isovalue is 0.0001 bohr^{-3}.

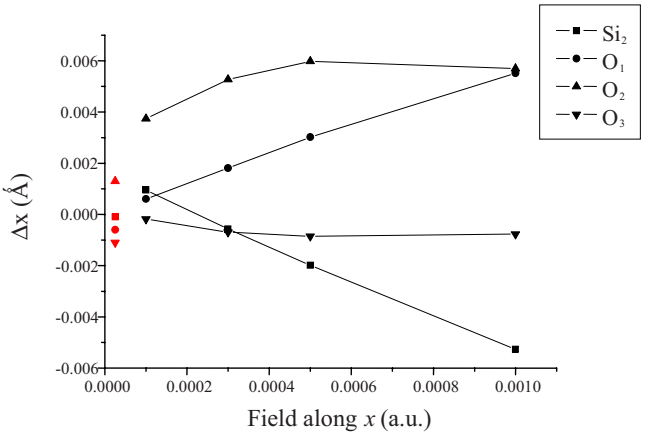

FIG. 4. (Color online) Calculated Si and O displacement (Å) along the a axis (direction of the field, $F_0\cong3\times10^{-5}$ a.u.) relative to electric field amplitude. Comparison with the available experimental data (Ref. 8).

TABLE III. Calculated angles in the unperturbed and perturbed structures for different electric field intensities (a.u.). $\Delta=\alpha(F_0\neq 0)-\alpha(F_0=0)$. Comparison with the experimental data (Ref. 8).

Angle α (deg)	$F_0=0$	$F_0=10^{-3}$	$F_0=5\times10^{-4}$	$F_0=10^{-4}$	Δ (10^{-3})	Δ (5×10^{-4})	Δ (10^{-4})	Δ (Expt. $\sim3\times10^{-5}$)
O_1-Si_1-O_{1a}	109.06	108.60	108.80	109.00	−0.46	−0.26	−0.06	−0.13
O_1-Si_1-O_3	110.48	110.63	110.58	110.51	0.15	0.10	0.03	0.21
O_1-Si_1-O_{3a}	108.54	108.66	108.61	108.56	0.12	0.07	0.02	−0.22
O_3-Si_1-O_{3a}	109.72	109.62	109.62	109.68	−0.10	−0.10	−0.04	0.28
O_{2a}-Si_{2a}-O_{3a}	110.48	110.85	110.71	110.56	0.37	0.23	0.08	0.11
O_{2a}-Si_{2a}-O_1	109.72	109.61	109.63	109.65	−0.11	−0.09	−0.07	−0.14
Si_{2a}-O_{3a}-Si_1	142.98	143.61	143.35	143.05	0.63	0.37	0.07	0.38
Si_2-O_{2a}-Si_{2a}	142.98	142.12	142.56	142.98	−0.86	−0.42	0.04	−0.40
Si_2-O_2-Si_{2a}	142.98	143.00	143.08	143.06	0.02	0.10	0.08	−0.40
Si_1-O_1-Si_{2a}	142.98	142.88	142.99	143.03	−0.10	0.01	0.05	0.15

Let us describe the phenomenon induced by the application of the external electric field. For an external electric field of 10^{-2} a.u., the results show larger induced electric dipoles on the oxygen atoms. These dipoles are aimed in the same orientation than the applied field and they are opposed against the depolarization field induced in the crystal. For an external electric field of 5×10^{-3} a.u., a similar effect on the oxygen atoms is found with a very weak effect on the silicon atoms. For an applied field of 10^{-3} a.u., a negligible effect is found on both silicon and oxygen atoms. Similar results were also found with the PS-PWGGA calculation. This shows that under 10^{-3} a.u., the electronic contribution completely disappears (the nuclei being fixed) and that the effect of the macroscopic field of 28.8 kV/cm ($\cong5.6\times10^{-6}$ a.u.) used experimentally by Guillot *et al.*[8] for the relative variations in x-ray scattering intensity of high-order reflections, should not be due to electronic shell deformation.

3. Atomic displacements

Starting from the optimized lattice parameters for the unit cell, we have optimized the geometry of the quartz SiO_2 in the presence of the electric field, in order to study the atomic displacements. The AE-B3LYP approach has been then preferred to the PS-PWGGA one since the influence of core electrons is certainly important in the atomic displacements. Several applied electric field amplitudes were tested in the direction of the crystallographic *a* axis going from 10^{-3} to 10^{-4} a.u. (10^{-4} a.u. being the smallest field amplitude value used in our calculation to obtain accurate results without extreme conditions on the convergence). We must notice that this latter value of the displacement field corresponds to a theoretical macroscopic field

$$F=\frac{F_0}{\varepsilon}\cong\frac{10^{-4}}{5}\ \text{a.u.}$$

($\cong$100 kV/cm) which is still larger than the experimental one of Guillot *et al.* (28.8 kV/cm). $\varepsilon=4-5$ represents the static dielectric constant taken from Ref. 35.

The evolution of atomic displacements along the direction of the electric field direction as a function of its external amplitude is reported in Fig. 4. It shows a quasilinear evolution of the displacements of Si_2, O_1, and O_3 atoms and a large curve for O_2 (with respect to Si_1) as a function of the applied electric field amplitude. For both O_1 and O_3 atoms bounded to Si_1, the displacements clearly converge on zero for an external field equal to zero while they seem to tend to a nonzero value (around 0.002 Å) for both Si_2 and O_2 atoms which are not directly bounded to Si_1. This gives the error bar of our calculated displacements $\cong$0.001 Å. The values

TABLE IV. Calculated angles between the Si-O bonds and the electric field direction for different amplitudes (a.u.). $\Delta=\alpha(F_0\neq 0)-\alpha(F_0=0)$. Comparison with the experimental data (Ref. 8).

Angle α (deg)	$F_0=0$	$F_0=10^{-3}$	$F_0=5\times10^{-4}$	$F_0=10^{-4}$	Δ (10^{-3})	Δ (5×10^{-4})	Δ (10^{-4})	Δ (Expt. $\sim3\times10^{-5}$)
Si_1-O_1	54.52	54.30	54.40	54.49	−0.22	−0.12	−0.03	−0.07
Si_1-O_{1a}	54.52	54.30	54.40	54.49	−0.22	−0.12	−0.03	−0.07
Si_1-O_3	54.86	54.81	54.81	54.84	−0.05	−0.05	−0.02	0.14
Si_1-O_{3a}	54.86	54.81	54.81	54.84	−0.05	−0.05	−0.02	0.14
Si_{2a}-O_2	24.82	24.86	24.92	24.93	0.04	0.10	0.11	−0.50
Si_{2a}-O_{2a}	52.04	52.47	52.21	51.99	0.43	0.17	−0.05	−0.01
Si_{3a}-O_{3a}	70.89	70.69	70.82	70.93	−0.20	−0.07	0.04	−0.05
Si_{2a}-O_1	87.73	87.79	87.70	87.68	0.06	−0.03	−0.05	−0.02

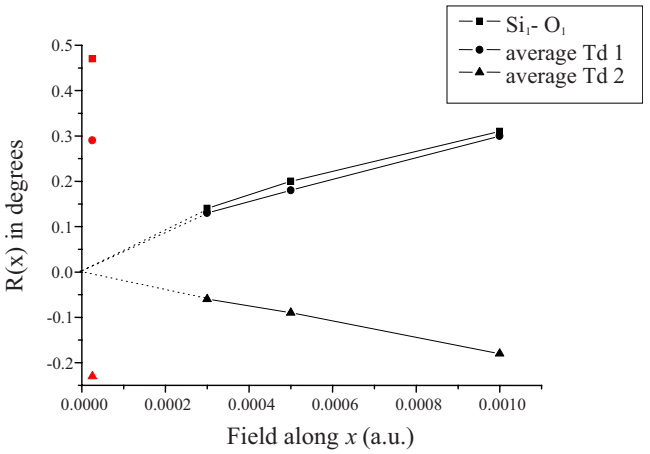

FIG. 5. (Color online) Calculated overall rotations (in degrees) around the electric field direction (*a* axis) relative to electric field amplitude ($F_0 \cong 3 \times 10^{-5}$ a.u.). Comparison with the experiment (Ref. 8).

pointed out at $F_0 \cong 3 \times 10^{-5}$ a.u. are the experimental results obtained by Guillot *et al.*[8] for a macroscopic field F of 28.8 kV/cm. For an external field F_0 of 10^{-4} a.u. (i.e., three times stronger than the experimental one), it is interesting to note that our results for the calculated displacements are roughly similar to those of the experiment but shifted of 0.001 Å along the field direction (*a* axis).

Along the directions perpendicular to the applied external field, a quasilinear evolution not reported in this work is found for the displacements of Si_2, O_1, O_2, and O_3 atoms with respect to Si_1. However, our results for the perpendicular displacements are found in the same order of magnitude as those along the *a* direction. This is not in good agreement with the experimental measurements given in Ref. 8 showing that the atomic displacements along the directions perpendicular to the field are much larger than those obtained along the electric field (*a* axis).

a. O-Si-O angle. Since the geometrical structure is formed of corner-sharing SiO_4 tetrahedra, its deformation in the presence of an external electric field can be better analyzed by angle variations than by perpendicular displacements of Si and O atoms. Following this, we have calculated the O-Si-O angles in the unperturbed and perturbed structures and the angle between the Si-O bonds and the electric field direction. Table III shows the results for the O-Si-O angles for both unperturbed and perturbed structures at the AE-B3LYP level. The results show smaller variation in angles compared to experimental data. Table IV reports the values for the angle between the Si-O bonds of two independent tetrahedra centered at Si_1 and Si_{2a} and the electric field direction. The same very small order of magnitude as in the experiment is found.

b. Overall rotation. We have also calculated the overall rotations of the Si-O bonds in each tetrahedron around the electric field direction (*a* axis) as in Ref. 8. Figure 5 presents the evolution of the overall rotations of the Si_1-O_1 bond and both tetrahedra (centered at Si_1 and Si_{2a}) around the electric field direction as a function of its amplitude. Only the rotations around the electric field direction are analyzed, those around both directions perpendicular to the field being negligible as in Ref. 8. Figure 5 shows a linear evolution of the rotations as a function of the applied field amplitude. If the same order Si-O_1 > average Td_1 > 0 > average Td_2 is obtained, the calculated rotations are found to be smaller than the experimental values (with a factor 2–4 for an external electric field $F_0 = 3 \times 10^{-4}$ a.u. ten times larger than the experimental one, for example).

IV. CONCLUSION

The response properties of α-quartz SiO_2 to an external static electric field have been investigated in the framework of the DFT in order to highlight the comparison with the experimental measurements obtained by Guillot *et al.*,[8] and to clarify the electronic and structural contributions to the piezoelectric properties.

Two functionals (B3LYP and PWGGA) and two kinds of basis sets (PS and AE) are used. First, the determination of the direct gap, the high-frequency dielectric constant, and the elastic and piezoelectric tensors of α quartz is done. A comparison with other theoretical and experimental results confirms the accuracy of our calculations particularly when the AE-B3LYP and PS-PWGGA methods are used.

Then, differences of electron-density maps of the quartz at fixed geometry in presence of an external field have been plotted showing that the deformation of the electron cloud could be neglected for a field modulus less than 10^{-3} a.u.. It confirms that the variations in (large angle) structure factors observed in Ref. 8 when a macroscopic field of 28.8 kV/cm ($\cong 5.6 \times 10^{-6}$ a.u.) is applied to the quartz α are mainly due to the atomic displacements aroused by the field, with a negligible electronic contribution.

Our results for the nuclear displacements along the direction of the electric field (*a* axis) are found to be similar to those obtained by Guillot *et al.*[8] from structure factors measurements when the all-electron basis set is used (AE-B3LYP method). On the contrary, for perpendicular displacements, the theoretical results are found in the same order of magnitude as those along the *a* direction, which is not in good agreement with Ref. 8 where atomic displacements along the directions perpendicular to the field are much larger than those obtained along the electric field (*a* axis). In the present work, rotations of the Si-O bonds around the electric field direction (*a* axis) in the two independent tetrahedra, are smaller than those deduced from the experiment.

This work will be used as a basis model to treat other typical compounds which exhibit strong piezoelectric properties such as $AlPO_4$, $FePO_4$, $GaPO_4$, and $GaAsO_4$.

ACKNOWLEDGMENTS

It is a pleasure to acknowledge continued discussions with Roberto Dovesi and Loredana Valenzano who also allowed us to use the new version of CRYSTAL for the gradient of the perturbation saw-tooth potential.

*Corresponding author. FAX: 33 5 59 40 78 62; michel.rerat@univ-pau.fr

[1] K. J. Kingma, C. Meade, R. J. Hemley, H. K. Mao, and D. R. Veblen, Science **259**, 666 (1993); K. J. Kingma, R. J. Hemley, H. K. Mao, and D. R. Veblen, Phys. Rev. Lett. **70**, 3927 (1993); L. E. McNeil and M. Grimsditch, *ibid.* **72**, 1301 (1994).

[2] E. G. Ponyatovsky and O. I. Barkalov, Mater. Sci. Rep. **8**, 147 (1992).

[3] E. Gregoryanz, R. J. Hemley, H.-K. Mao, and P. Gillet, Phys. Rev. Lett. **84**, 3117 (2000); M. H. Muser and P. Schoffel, *ibid.* **90**, 079701 (2003); E. Gregoryanz, R. J. Hemley, H. K. Mao, R. E. Cohen, and P. Gillet, *ibid.* **90**, 079702 (2003).

[4] L. E. McNeil and M. Grimsditch, Phys. Rev. Lett. **68**, 83 (1992).

[5] R. Tarumi, K. Nakamura, H. Ogi, and M. Hirao, J. Appl. Phys. **102**, 113508 (2007).

[6] H. Ogi, T. Ohmori, N. Nakamura, and M. Hirao, J. Appl. Phys. **100**, 053511 (2006).

[7] O. Cambon, J. Haines, G. Fraysse, J. Détaint, B. Capelle, and A. Van der Lee, J. Appl. Phys. **97**, 074110 (2005).

[8] R. Guillot, P. Fertey, N. K. Hansen, P. Allé, E. Elkaïm, and C. Lecomte, Eur. Phys. J. B **42**, 373 (2004).

[9] D. W. McComb and A. Howie, Nucl. Instrum. Methods Phys. Res. B **96**, 569 (1995).

[10] See the electronic address, http://www. impex-hightech.de/ of Impex High Tech GmbH.

[11] L. Levien, C. T. Prewitt, and D. Weidner, Am. Mineral. **65**, 920 (1980).

[12] H. Kimizuka, S. Ogata, J. Li, and Y. Shibutani, Phys. Rev. B **75**, 054109 (2007).

[13] N. Choudhury and S. L. Chaplot, Phys. Rev. B **73**, 094304 (2006).

[14] L. E. Ramos, J. Furthmüller, and F. Bechstedt, Phys. Rev. B **69**, 085102 (2004).

[15] B. Holm and R. Ahuja, J. Chem. Phys. **111**, 2071 (1999).

[16] M. Levy, H. E. Bass, and R. R. Stern, *Handbook of Elastic Properties of Solids, Liquids and Gases* (Academic, San Diego, 2001), Vol. II.

[17] A. Meissner, Zeitschrift Techn Physik. **2**, 74 (1927).

[18] U. Pietsch, J. Stahn, J. Davaasambuu, and A. Pucher, J. Phys. Chem. Solids **62**, 2129 (2001).

[19] J. Davaasambuu, Ph.D. thesis, University of Potsdam, 2003.

[20] J. Davaasambuu, A. Pucher, K. Kochim, and U. Pietsch, Europhys. Lett. **62**, 834 (2003).

[21] S. C. Abrahams, Acta Crystallogr., Sect. A: Cryst. Phys., Diffr., Theor. Gen. Crystallogr. **46**, 297 (1975).

[22] V. R. Saunders, R. Dovesi, C. Roetti, R. Orlando, C. M. Zicovich-Wilson, F. Pascale, N. M. Harrison, K. Doll, B. Civalleri, I. J. Bush, P. D'Arco, and M. Llunell, In CRYSTAL06 *User's Manual* University of Torino, Torino, 2006 (http://www.crystal.unito.it).

[23] J. P. Perdew and Y. Wang, Phys. Rev. B **33**, 8800 (1986).

[24] J. P. Perdew and Y. Wang, Phys. Rev. B **40**, 3399 (1989).

[25] J. P. Perdew and Y. Wang, Phys. Rev. B **45**, 13244 (1992).

[26] A. D. Becke, Phys. Rev. A **38**, 3098 (1988).

[27] C. Lee, W. Wang, and R. G. Parr, Phys. Rev. B **37**, 785 (1988).

[28] L. Valenzano, F. J. Torres, K. Doll, F. Pascale, C. M. Zicovich-Wilson, and R. Dovesi, Z. Phys. Chem. **220**, 893 (2006).

[29] R. Nada, C. R. A. Catlow, R. Dovesi, and C. Pisani, Phys. Chem. Miner. **17**, 353-362 (1990).

[30] P. Durand and J. C. Barthelat, Theor. Chim. Acta **38**, 283 (1975).

[31] L. H. Jolly, Ph.D. thesis, Université Pierre et Marie Curie, 1993.

[32] C. Darrigan, M. Rérat, G. Mallia, and R. Dovesi, J. Comput. Chem. **24**, 1305 (2003).

[33] R. Resta, Rev. Mod. Phys. **66**, 899 (1994).

[34] J. Muscat, A. Wander, and N. M. Harrison, Chem. Phys. Lett. **342**, 397 (2001).

[35] A. De and K. V. Rao, J. Mater. Sci. **23**, 661 (1988).